Organic Electronics 73 (2019) 327–331

Contents lists available at ScienceDirect

Organic Electronics

journal homepage: www.elsevier.com/locate/orgel

Effects of CsPbBr3 nanocrystals concentration on electronic structure and surface composition of perovskite films

Yuquan Liu[a], Huachao Zai[b], Haipeng Xie[a,*], Baoxing Liu[a], Shitan Wang[a], Yuan Zhao[a], Dongmei Niu[a], Han Huang[a], Qi Chen[b], Yongli Gao[a,c]

[a] Hunan Key Laboratory of Super-microstructure and Ultrafast Process, School of Physics and Electronics, Central South University, Changsha, Hunan, 410012, China
[b] School of Materials Science and Engineering, Beijing Institute of Technology, Beijing, 100081, China
[c] Department of Physics and Astronomy, University of Rochester, Rochester, 14627, USA

ARTICLE INFO

Keywords:
$CsPbBr_3$ NCs
Perovskite films
Electronic structure
Photoemission spectroscopy

ABSTRACT

The electronic structure and surface composition of perovskite films after incorporation of different concentration of $CsPbBr_3$ nanocrystals (NCs) have been investigated with ultraviolet photoelectron spectroscopy (UPS) and X-ray, and angle-resolved photoelectron spectroscopy (XPS, AR-XPS). The electronic structure, surface composition and morphology of perovskite film have been changed through the interaction between $CsPbBr_3$ NCs and perovskite film. The band can be shifted upward by in incorporation of $CsPbBr_3$ NCs and it is independent of the concentration of $CsPbBr_3$ NCs. The surface component and its distribution can be adjusted by changing the concentration of $CsPbBr_3$ NCs and the proper concentration of $CsPbBr_3$ NCs would improve the stoichiometric ratio of perovskite film.

1. Introduction

Organic-inorganic hybrid perovskite solar cells (PSCs) have attracted intensive interests recently due to their advantages, such as remarkably high absorption, long charge carrier diffusion lengths and low cost [1–6]. The most attractive and representative perovskites are methylammonium lead halides ($CH_3NH_3PbX_3$, denoted as $MAPbX_3$), which were discovered in 2009 as sensitizers in dye-sensitized solar cells (DSSCs) [7]. Recently, a power conversion efficiency (PCE) of 23.3% was certified by the National Renewable Energy Laboratory [8]. In 2014, Grätzel et al. demonstrated that a perovskite-sensitized photovoltaic device based on mixture of formamidinium ($CHNH_3^+$, FA) and methylammonium cations ($CH_3NH_3^+$, MA), which increases the short-circuit current, meanwhile the open circuit voltage is not reduced [9]. In 2018, highly efficient triple cation PSCs were successfully fabricated by the combinations of three kinds of cations (FA, MA, Cs) [10]. To obtain high power conversion efficiency (PCE), many efforts have been made in the context of interface engineering, such as optimizing absorber materials, film fabrication and interface engineering [11–16]. Zhou et al. reported that a power conversion efficiency of 19.3% were obtained by doping the TiO_2 ETL to enhance its carrier concentration and modifying the ITO electrode to reduce its work function [14]. Zuo et al. demonstrated that proper interfacial interactions can significantly reduce trap state density and facilitate the interfacial charge transfer [15]. Wolff et al. performed a study that a power conversion efficiency of 19.4% were realized by inserting an ultrathin layer of an insulating polymer between the active perovskite and the fullerene [16]. Snaith.et al. demonstrated the feasibility of achieving > 25%-efficient four-terminal tandem cells by a mixed-cation lead mixed-halide perovskite absorber for tandem solar cells [17].

The $CsPbBr_3$ has been well-applied in PSCs and achieved great success in PSCs due to its excellent optoelectronic properties. To obtain high power conversion efficiency, Zhou et al. reported a photon management study, in which $CsPbBr_3$ nanowires were applied on top of the perovskite absorber to achieve localized gratings for an improved fluorescence effect [18]. Recently, Chen et al. demonstrate modification of perovskite absorber by incorporation of $CsPbBr_3$ nanocrystals ($CsPbBr_3$ NCs) which led to significant enhancement in photovoltaic performance and the power conversion efficiency (PCE) increased first and then decreased with $CsPbBr_3$ NCs increased from 0 to 3 mg/mL due to the poor film morphology that originated from the incompatibility of the deposition method (spin-coating) used.[19] However, some basic problems remain still unsolved, such as the precise relation between the surface composition of perovskite films and the concentration of $CsPbBr_3$ NCs, and the distribution of chemical components in perovskite films modification of different concentration of $CsPbBr_3$ NCs is

* Corresponding author.
E-mail address: xiehaipeng@csu.edu.cn (H. Xie).

https://doi.org/10.1016/j.orgel.2019.06.040
Received 20 March 2019; Received in revised form 17 June 2019; Accepted 25 June 2019
Available online 26 June 2019

yet to be achieved.

In this paper, the goal is to deepen our understanding of the interaction mechanism between $CsPbBr_3$ NCs and perovskite films. We report our systematic investigations on the electronic structure, surface composition, and the component distribution of the $FA_{0.85}MA_{0.15}Pb(I_{0.85}Br_{0.15})_3$ films fabricated with different concentration of $CsPbBr_3$ NCs using ultraviolet photoelectron spectroscopy(UPS), X-ray, and angle-resolved X-ray photoelectron spectroscopy (XPS, AR-XPS), atomic force microscopy(AFM). The UPS shows that the modification of $CsPbBr_3$ NCs in perovskite film can affect its work function and the energy level alignment, and it is independent of the concentration of $CsPbBr_3$ NCs. The core level shifts of the perovskite films and the appearance of a new peak observed by XPS indicate that $CsPbBr_3$ NCs not only change electronic structure but also change the surface chemical composition of perovskite film. The optimal stoichiometric ratio of the perovskite film has been obtained after incorporation of 2 mg/mL $CsPbBr_3$ NCs. These investigations provide explanation of microscopic level to help improve the device performance.

2. Experimental

The $FA_{0.85}MA_{0.15}Pb(I_{0.85}Br_{0.15})_3$ films and $CsPbBr_3$ NCs were prepared according to the reported procedure,[14] The FAI (1.02 M), PbI_2 (1.02 M), MABr (0.18 M) and $PbBr_2$ (0.18 M) were dissolved in mixed solvent of N, *N*-dimethylformamide (DMF) and Dimethyl sulfoxide (DMSO)with a volume ratio of 4:1. Then the mixed solvent was spun coated onto ITO substrate at a rate of 3000 rpm for 30 s. Chlorobenzene (CB) or CB/$CsPbBr_3$ NCs (300 μL) was dropped on the spinning substrate during the spin-coating step at 10 s before the end of the procedure. The substrates were then immediately transferred on a hot plate and heated at 130 °C for 15 min. The average size of the monodisperse $CsPbBr_3$ NCs is 12 nm and the characteristic interplanar distance of the $CsPbBr_3$ is 0.58 nm [19].

The four kinds of $FA_{0.85}MA_{0.15}Pb(I_{0.85}Br_{0.15})_3$ films modified by different concentration of $CsPbBr_3$ NCs were sent into the characterization chamber for UPS and XPS measurements. The UPS was measured with a microwave UV Light Source (He I, $h\nu = 21.22$ eV) and XPS with a monochromatic Microfocus X-ray Source (Al K_α, $h\nu = 1486.7$ eV). The UV light spot is about 1 mm in diameter and a total energy resolution of 70 meV was selected for the UPS measurements as determined from the Fermi edge of Au. For XPS, the resolution of the spectrometer was chosen to be 0.65 eV with the pass energy setting of 40 eV. The binding energies of all UPS and XPS spectra were calibrated and referenced to the Fermi level (E_F) of the sample [20–23]. The morphology of the perovskite films were measured ex situ using an Agilent 5500AFM/SPM system. All measurements were taken at room temperature.

3. Results and discussion

In Fig. 1, the UPS spectra of the perovskite films are presented as a function of the $CsPbBr_3$ NCs concentration. For visual clarity, we normalized all the spectra to the same height. The UPS data of the cut-off region are shown in Fig. 1a. The work function (WF) was obtained by the energy difference between the secondary cut-off and the E_F of the system. For as-grown perovskite film, the WF is 3.75 eV which is a little smaller than other group's reports [24]. After incorporation of $CsPbBr_3$ NCs, the WFs increase to 3.80 eV and keep unchanged with the change of the concentration of $CsPbBr_3$ NCs. Fig. 1b presents the UPS data of the valence band (VB) regions, we found that the valence band maximum (VBM) shifts toward to the Fermi energy (E_F) after incorporation of $CsPbBr_3$ NCs. The VBM of as-grown perovskite film is observed to be 1.54 eV below the E_F, which shows an *n*-type film and the band gap of perovskite film is 1. 62 eV [19]. Then the VBM shifts toward to 1.36 eV below the E_F after incorporation of $CsPbBr_3$ NCs and it remains unchanged with the change of the concentration of $CsPbBr_3$ NCs, indicating that the VBM of perovskite film is modified by the incorporation of $CsPbBr_3$ NCs but almost not influenced by the concentration of the NCs. Shown in Fig. 1c is the energy-level diagram of perovskite film before and after $CsPbBr_3$ NCs modified. We can find that a band shift appears after incorporation of $CsPbBr_3$ NCs, which is beneficial to improve device performance, as previously reported.[19]

In order to gain a good understanding of the electronic structure of perovskite films after incorporating different concentrations of $CsPbBr_3$ NCs, we used XPS to investigate further the chemical characteristics. Presented in Fig. 2 are the XPS spectra of C 1s, N 1s, I $3d_{5/2}$, Br 3d and Pb $4f_{7/2}$ of perovskite films fabricated with different concentration of $CsPbBr_3$ NCs. The binding energy (BE) of each element at the surface of the perovskite film was calibrated with reference to the amorphous carbon C 1s core level of 284.5 eV. We find that the BE of I $3d_{5/2}$, Pb $4f_{7/2}$, C 1s, Br 3d, and N 1s core level shift to low BE after incorporation of $CsPbBr_3$ NCs and the total shift is about 0.32 eV, almost following the same shift trend observed by the UPS spectra (Fig. 1). With the increasing of the concentration of $CsPbBr_3$ NCs, the core level keeps unchanged. Chen et al. reported that the depth-dependent distribution of $CsPbBr_3$ NCs in the modified perovskite film due to the sample surface and bulk are closed to the $CsPbBr_3$ NCs and PVSK respectively.[19] The depth of $CsPbBr_3$ NCs incorporation in the perovskite films is limited and it is beyond the detection depth of UPS and XPS (the detection limit is about 10 nm). Thus, the VBM and core level keep unchanged with the increasing of the concentration of $CsPbBr_3$ NCs (as shown in Figs. 1 and 2). The I $3d_{5/2}$ core level include a single peak as shown in Fig. 2a, which can be assigned to lattice I components in $FA_{0.85}MA_{0.15}Pb(I_{0.85}Br_{0.15})_3$ films before and after incorporation of $CsPbBr_3$ NCs. As shown in Fig. 2b, the Pb $4f_{7/2}$ core level include only one peak which is located at ca. 137.81 eV after incorporation of $CsPbBr_3$ NCs. Literature reported that the Pb component in $CsPbBr_3$ is located at 138.30–139.20 eV [25,26]. It is higher than the test results, indicated that the Pb $4f_{7/2}$ core level located at ca. 137.81 eV come primarily from the Pb component in $FA_{0.85}MA_{0.15}Pb(I_{0.85}Br_{0.15})_3$ films after incorporation of $CsPbBr_3$ NCs. This indicated that traces of $CsPbBr_3$ NCs incorporation into $FA_{0.85}MA_{0.15}Pb(I_{0.85}Br_{0.15})_3$ films and the content of Pb in the incorporation of $CsPbBr_3$ NCs is below the XPS detection limit. Similarly, no Cs 3d signals has been detected due to the lower content $CsPbBr_3$ NCs in modified perovskite films.[19] In Fig. 2c, the C 1s core level includes more than one peaks for all perovskite films. The C 1s peaks centered on 284.50 and 288.06 eV are assigned to amorphous carbon and carbons in the formamidine of the $FA_{0.85}MA_{0.15}Pb(I_{0.85}Br_{0.15})_3$ film, respectively. The methyl carbons peak centered on ca. 285.9 eV has been reported in the literature which appear to be partially overlapping in the spectra (Fig. 2c). Similar to Pb, the Br 3d core level located at ca. 68.96 eV which is lower or higher than that of the previous report.[25, 26] Furthermore, we calculated the core level difference between Pb 4f and Br 3d in ref. 25, 26 is about 70 eV, which is higher than that of $FA_{0.85}MA_{0.15}Pb(I_{0.85}Br_{0.15})_3$ film in here (the value is about 68.85 eV). Thus, the Pb 4f and Br 3d in Fig. 2 can be attributed to the lattice Pb and Br components in $FA_{0.85}MA_{0.15}Pb(I_{0.85}Br_{0.15})_3$ film. As shown in Fig. 2e, f, it is found that the N 1s core level located at ca. 399.95 and 401.70 eV which can be assigned to the N signal in FA and MA respectively before and after incorporation of $CsPbBr_3$ NCs. After incorporation of $CsPbBr_3$ NCs, the N 1s core level shift to lower binding energy. As shown in Fig. 2f, the relative content of N components in MA increased and the FA/MA ratios are ca. 14.27, 8.63, 6.18, 8.36 respectively, corresponding to the $CsPbBr_3$ NCs concentration increases from 0 to 3 mg/mL. The ratio of FA/MA decreases and reaches the minimum value when the concentration of $CsPbBr_3$ NCs increase to 2 mg/mL, which is close to the stoichiometric ratio of $FA_{0.85}MA_{0.15}Pb(I_{0.85}Br_{0.15})_3$ film. Further increases the $CsPbBr_3$ NCs concentration, the ratio of FA/MA has significantly increased. It is indicating that the stoichiometric ratio of $FA_{0.85}MA_{0.15}Pb(I_{0.85}Br_{0.15})_3$ film can be affected by incorporation of $CsPbBr_3$ NCs and the proper concentration of $CsPbBr_3$ NCs would improve the stoichiometric ratio of

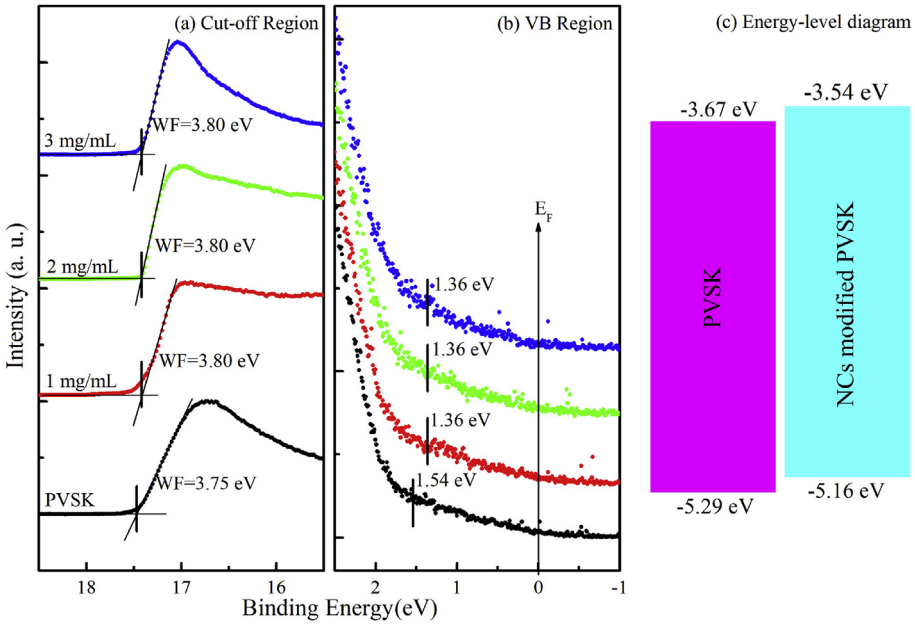

Fig. 1. UPS spectra of (a) cut-off region and(b) VB region near the Fermi level as a function of the $CsPbBr_3$ NCs concentration. PVSK corresponding to as-grown perovskite film. (c) Energy-level diagram of perovskite film before and after $CsPbBr_3$ NCs modified.

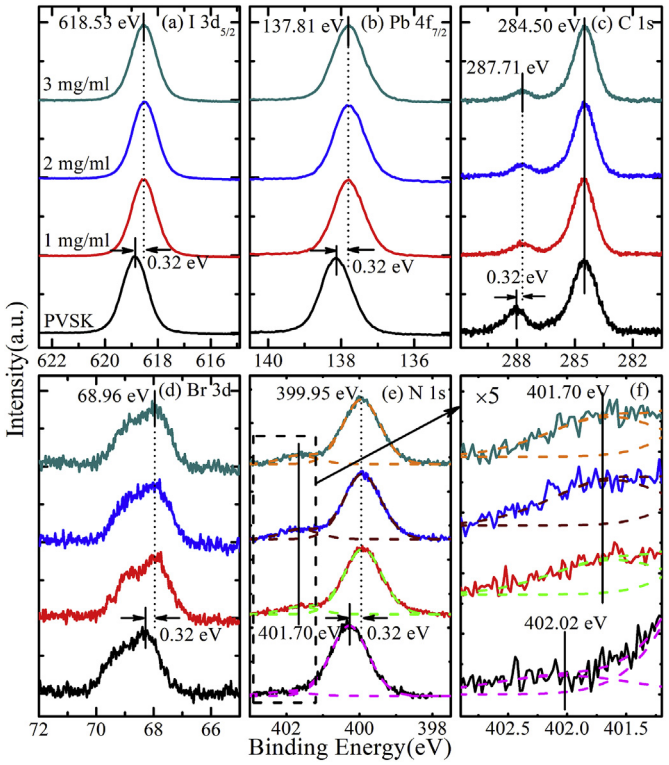

Fig. 2. XPS spectra of (a) I $3d_{5/2}$, (b) Pb $4f_{7/2}$ (c) C1s (d)Br 3d (e) N 1s for perovskite films fabricated with different concentration of $CsPbBr_3$ NCs in the dripping solvent (f) The × 5 magnified image of the dashed box in (e).

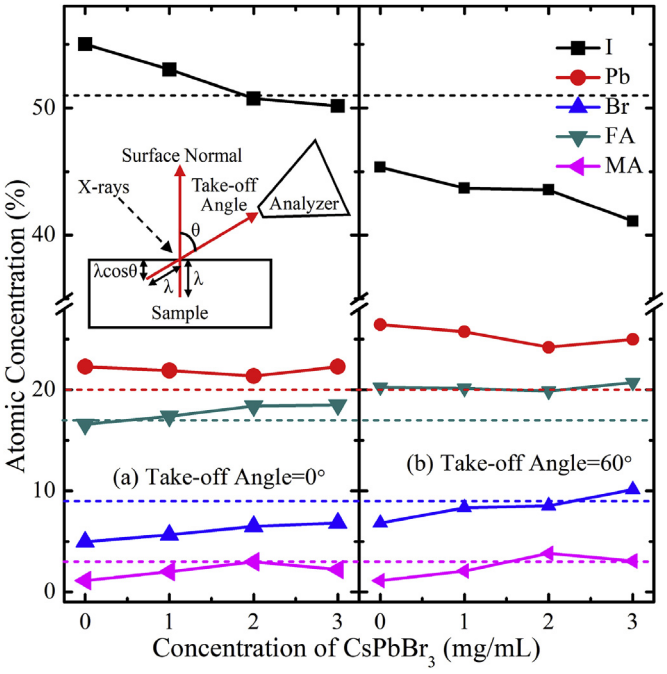

Fig. 3. Atomic concentration of all components in the perovskite films as a function of the concentration of $CsPbBr_3$ NCs for (a) the take-off angle is 0^0 (b) the take-off angle is 60^0. The inset is the measurement geometry of AR-XPS. The dash line corresponds to the stoichiometric ratio of $FA_{0.85}MA_{0.15}Pb(I_{0.85}Br_{0.15})_3$ film and the different colors correspond to the corresponding element.

perovskite film.

To further analyze the elemental composition and the distribution of all components in the bulk and surface regions of the perovskite films before and after the incorporation of different concentration of $CsPbBr_3$ NCs. XPS and AR-XPS is used for the perovskite films fabricated with different concentration of $CsPbBr_3$ NCs in the dripping solvent. As shown in Fig. 3, the atomic concentrations of all components are plotted as a function of the concentration of $CsPbBr_3$ for the take-off angle is 0^0 and the take-off angle is 60^0. The measurement geometry of AR-XPS is shown in the inset of Fig. 3a. The probing depth is λcosθ, where λ is the mean diffusion length of electron in perovskite film, decreases with the increase of takeoff angle, indicating that the larger takeoff angle can be used to reflect the content composition of film closer to the surface [27,28].

Shown in Fig. 3a are the elemental composition in $FA_{0.85}MA_{0.15}Pb(I_{0.85}Br_{0.15})_3$ films with different concentration of $CsPbBr_3$ NCs in the dripping solvent. The percentage of I decreased while the percentage of

Br gradually increased with the increase of concentration of $CsPbBr_3$ NCs, that's because of $CsPbBr_3$ NCs incorporation which increase the content of Br. The percentage of amino FA remain nearly unchanged and that of the MA increases first and then decreases as the increase of concentration of $CsPbBr_3$ NCs. For the as-grown perovskite film, we can find that the I content is about 55% which is higher than that of the $FA_{0.85}MA_{0.15}Pb(I_{0.85}Br_{0.15})_3$ film, as shown in Fig. 3a. With the increasing of concentration of $CsPbBr_3$ NCs, the I content decreases and reaches the minimum value (about 50%) in the $CsPbBr_3$ NCs concentration of 3 mg/mL. For the 2 mg/mL $CsPbBr_3$ NCs, the I content is about 50.6% which is close to the stoichiometric ratio of $FA_{0.85}MA_{0.15}Pb(I_{0.85}Br_{0.15})_3$ film, and the Pb, Br, FA, MA content are ca. 21.4%, 6.5%, 18.4%, 2.9% respectively. It is relatively close to the stoichiometric ratio of $FA_{0.85}MA_{0.15}Pb(I_{0.85}Br_{0.15})_3$ film after modification of 2 mg/mL $CsPbBr_3$ NCs.

Comparing Fig. 3a with 3b (0^0 and 60^0 corresponding to the bulk and surface regions respectively), we can find that the I fraction decreases slightly as the takeoff angle increases, indicating that there is more I in the bulk than in the surface region of the perovskite film before and after the incorporation of $CsPbBr_3$ NCs. The Pb fraction increase slightly as the takeoff angle increases, indicating that there is more Pb in the surface than in the bulk region of the perovskite film. The amounts of Br, FA and MA remain nearly unchanged as the takeoff angle increases, showing a homogeneous distribution in the perovskite film.

To highlight the relative distribution of all components in the perovskite films, we plot the relative depths of all chemical components in the perovskite film fabricated with different concentration of $CsPbBr_3$ NCs by using the AR-XPS data, as shown in Fig. 4. This plot uses the relative sensitivity of each chemical component with respect to the takeoff angle, which allows sorting the components as a function of depth. The relative depth is calculated from the ratio of relative intensities, $\ln(I_{surface}/I_{bulk})$ for each component, where $I_{surface}$ represents the intensity at takeoff angle of 60̊ and I_{bulk} represents the intensity at takeoff angle of 0̊ [29]. For the original perovskite film, it is observed that the Br and FA components have smaller relative depth, the I and MA component have greater relative depth, and the Pb component has a moderate relative depth as shown in Fig. 5a. Then, the relative depths of the Pb component have reduced slightly and MA component have greater relative depth after modification of 1 mg/mL $CsPbBr_3$ NCs as shown in Fig. 4b. Furthermore, the relative depth of the MA has reduced slightly while FA component have increased slightly after modification of 2 mg/mL $CsPbBr_3$ NCs as shown in Fig. 4c. However, there is slight change in relative depth of FA and MA components after modification of 3 mg/mL $CsPbBr_3$ NCs as shown in Fig. 4d. These changes are related to interaction between $CsPbBr_3$ NCs and perovskite film, which have an influence on the surface component and its distribution.

The surface morphologies of the perovskite films fabricated with different concentration of $CsPbBr_3$ NCs were investigated with AFM. As shown in Fig. 5, the grain size of perovskite decreased as the concentration of $CsPbBr_3$ NCs increased, while the density of the film increased. The surface morphology changed obviously as the concentration reached 3 mg/mL.

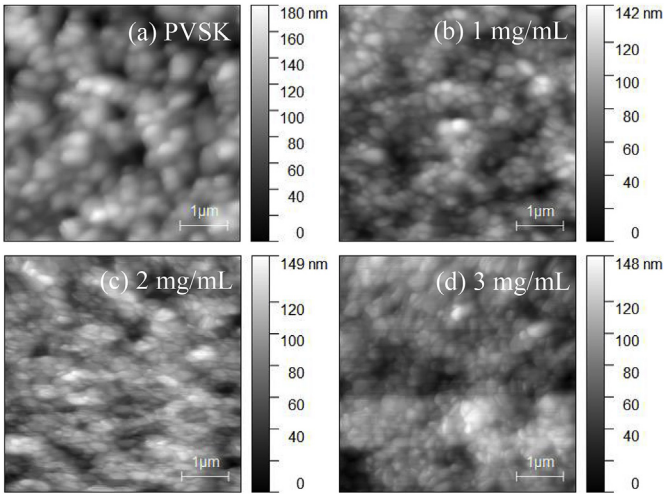

Fig. 5. AFM morphology images of perovskite film fabricated with different concentration of $CsPbBr_3$ NCs.

4. Conclusions

In summary, we have investigated the electronic structure, surface composition and morphology of the $FA_{0.85}MA_{0.15}Pb(I_{0.85}Br_{0.15})_3$ films fabricated with different concentration of $CsPbBr_3$ NCs using UPS, XPS and AFM. It is found that the change of the concentration of $CsPbBr_3$ NCs would adjust the electronic structure and surface composition of perovskite films. An upward shift in valence band of the perovskite film is resulted by incorporating the $CsPbBr_3$ NCs and the shift is independent of the concentration of $CsPbBr_3$ NCs. The stoichiometric ratio of perovskite film also can be improved by incorporating the proper concentration of $CsPbBr_3$ NCs. These results provide a better understanding of the underlying mechanisms between the perovskite film and the concentration of the modified materials, which is useful to improve the performances of perovskite solar cells.

Acknowledgements

We thank the financial support by the National Key Research and Development Program of China (Grant Nos. 2017YFA0206602), the National Natural Science Foundation of China (Grant Nos. 11334014 and 51802355), and National Key Laboratory Open Project Foundation (Grant No. 165000001). H.X. acknowledges the support by the Natural Science Foundation of Hunan Province (Grant No. 2018JJ3625). Y.L.

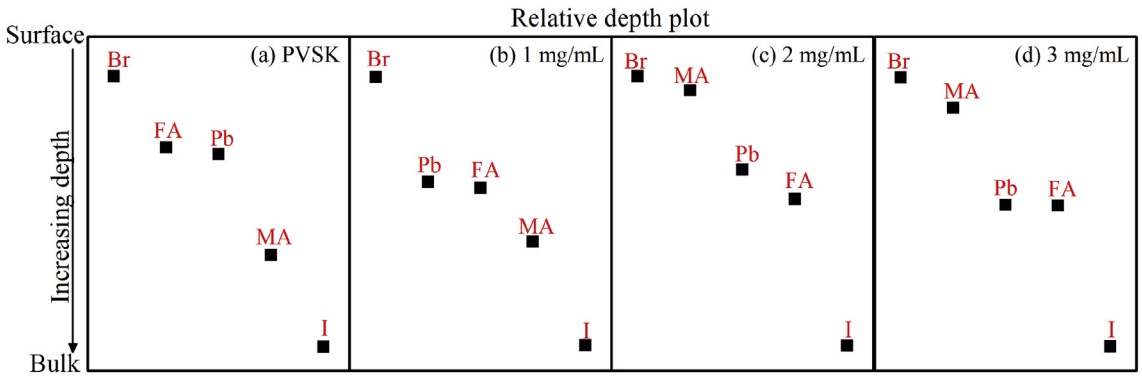

Fig. 4. Relative depth plot of chemical components for perovskite film fabricated with different concentration of $CsPbBr_3$ NCs.

acknowledges the Innovation Fund for Graduate Students of CSU (2018zzts349). Y. G. acknowledges the support from National Science Foundation (DMR-1903981 and 1903962).

References

[1] D.Q. Bi, W. Tress, M.I. Dar, P. Gao, J.S. Luo, C. Renevier, K. Schenk, A. Abate, F. Giordano, J.-P.C. Baena, et al., Efficient luminescent solar cells based on tailored mixed-cation perovskites, Sci. Adv. 2 (2016) e1501170https://doi.org/10.1126/sciadv.1501170.

[2] A. Abrusci, S.D. Stranks, P. Docampo, H.-L. Yip, A.K.-Y. Jen, H.J. Snaith, High-performance perovskite-polymer hybrid solar cells via electronic coupling with fullerene monolayers, Nano Lett. 13 (2013) 3124–3128 https://doi.org/10.1021/nl401044q.

[3] N.-G. Park, Organometal perovskite light absorbers toward a 20% efficiency low-cost solid-state mesoscopic solar cell, J. Phys. Chem. Lett. 4 (2013) 2423–2429 https://doi.org/10.1021/jz400892a.

[4] M.Z. Liu, M.B. Johnston, H.J. Snaith, Efficient planar heterojunction perovskite solar cells by vapour deposition, Nature 501 (2015) 395–398 https://doi.org/10.1038/nature12509.

[5] S.D. Stranks, G.E. Eperon, G. Grancini, C. Menelaou, M.J.P. Alcocer, T. Leijtens, L.M. Herz, A. Petrozza, H.J. Snaith, Electron-hole diffusion lengths exceeding 1 micrometer in an organometal trihalide perovskite absorber, Science 342 (2013) 341–344 https://doi.org/10.1126/science.1243982.

[6] F. Zhu, P.P. Zhang, X.J. Wu, L.M. Fu, J.P. Zhang, D.S. Xu, The origin of higher open-circuit voltage in Zn-doped TiO_2 nanoparticle-based dye-sensitized solar cells, ChemPhysChem 13 (2012) 3731–3737 https://doi.org/10.1002/cphc.201200362.

[7] A. Kojima, K. Teshima, Y. Shirai, T. Miyasaka, Organometal halide perovskites as visible-light sensitizers for photovoltaic cells, J. Am. Chem. Soc. 131 (2009) 6050–6051 https://doi.org/10.1021/ja809598r.

[8] https://www.nrel.gov/pv/assets/pdfs/pv-efficiencies-07-17-2018.pdf.

[9] N. Pellet, P. Gao, G. Gregori, T.-Y. Yang, M.K. Nazeeruddin, J. Maier, M. Grätzel, Mixed-organic-cation perovskite photovoltaics for enhanced solar-light harvesting, Angew. Chem. 126 (2014) 3215–3221 https://doi.org/10.1002/ange.201309361.

[10] R. Zhang, D.T. Liu, Y.F. Wang, T. Zhang, X.L. Gu, P. Zhang, J. Wu, Z.D. Chen, Y.C. Zhao, S.B. Li, Theoretical lifetime extraction and experimental demonstration of stable cesium-containing tri-cation perovskite solar cells with high efficiency, Electrochim. Acta 265 (2018) 98–106 https://doi.org/10.1016/j.electacta.

[11] Y.Z. Wu, X.D. Yang, W. Chen, Y.F. Yue, M.L. Cai, F.X. Xie, E.B. Bi, A. Islam, L.Y. Han, Perovskite solar cells with 18.21% efciency and area over $1cm^2$ fabricated by heterojunction engineering, Nat. Energy. 1 (2016) 16148 https://doi.org/10.1038/nenergy.2016.148.

[12] J.-W. Xiao, C.B. Shi, C.X. Zhou, D.L. Zhang, Y.J. Li, Q. Chen, Contact engineering: electrode materials for highly efficient and stable perovskite solar cells, Sol. RRL. 1 (2017) 1700082 https://doi.org/10.1002/solr.201700082.

[13] W. Chen, Y.Z. Wu, Y.F. Yue, J. Liu, W.J. Zhang, X.D. Yang, H. Chen, E.B. Bi, I. Ashraful, M. Grätzel, et al., Efficient and stable large-area perovskite solar cells with inorganic charge extraction layers, Science 350 (2015) 944–948 https://doi.org/10.1126/science.aad1015.

[14] H.P. Zhou, Q. Chen, G. Li, S. Luo, T.-B. Song, H.-S. Duan, Z.R. Hong, J.B. You, Y.S. Liu, Y. Yang, Interface engineering of highly efficient perovskite solar cells, Science 345 (2014) 542–546 https://doi.org/10.1126/science.1254050.

[15] L.J. Zuo, Q. Chen, N.D. Marco, Y.-T. Hsieh, H.J. Chen, P.Y. Sun, S.-Y. Chang, H.X. Zhao, S.Q. Dong, Y. Yang, Tailoring the interfacial chemical interaction for high-efficiency perovskite solar cells, Nano Lett. 17 (2017) 269–275 https://doi.org/10.1021/acs.nanolett.6b04015.

[16] C.M. Wolff, F.S. Zu, A. Paulke, L.P. Toro, N. Koch, D. Neher, Reduced interface-mediated recombination for high open-circuit voltages in $CH_3NH_3PbI_3$ solar cells, Adv. Mater. 29 (2017) 1700159 https://doi.org/10.1002/adma.

[17] D.P. McMeekin, G. Sadoughi, W. Rehman, G.E. Eperon, M. Saliba, M.T. Hörantner, A. Haghighirad, N. Sakai, L. Korte, B. Rech, et al., A mixed-cation lead mixed-halide perovskite absorber for tandem solar cells, Science 351 (2016) 151–155 https://doi.org/10.1126/science.aad5845.

[18] Y.H. Chen, L. Li, Z.H. Liu, N. Zhou, Q. Chen, H.P. Zhou, Photon management for efficient hybrid perovskite solar cells via synergetic localized grating and enhanced fluorescence effect, Nano Energy 40 (2017) 540–549 https://doi.org/10.1016/j.nanoen.

[19] H.C. Zai, C. Zhu, H.P. Xie, Y.Z. Zhao, C.B. Shi, Z.X. Chen, X.X. Ke, M.L. Sui, C.F. Chen, J.S. Hu, et al., Congeneric incorporation of $CsPbBr_3$ nanocrystals in a hybrid perovskite heterojunction for photovoltaic efficiency enhancement, ACS Energy Lett 3 (2018) 30–38 https://doi.org/10.1021/acsenergylett.7b00925.

[20] L. Zhang, Y.G. Yang, H. Huang, L. Lyu, H. Zhang, N.T. Cao, H.P. Xie, Y.L. Gao, Thickness-dependent air-exposure-induced phase transition of CuPc ultrathin films to well-ordered one-dimensional nanocrystals on layered substrates, J. Phys. Chem. *C* 119 (2015) 4217–4223 https://doi.org/10.1021/jp512613z.

[21] H.P. Xie, H. Huang, N.T. Cao, C.H. Zhou, D.M. Niu, Y.L. Gao, Effects of annealing on structure and composition of LSMO thin films, Physica B 477 (2015) 14–19 https://doi.org/10.1016/j.physb.2015.07.032.

[22] P. Liu, X.L. Liu, L. Lyu, H.P. Xie, H. Zhang, D.M. Niu, H. Huang, C. Bi, Z.G. Xiao, J.S. Huang, Y.L. Gao, Interfacial electronic structure at the $CH_3NH_3PbI_3$/MoOx interface, Appl. Phys. Lett. 106 (2015) 193903 https://doi.org/10.1016/j.physb.2015.07.032.

[23] H.P. Xie, D.M. Niu, L. Lyu, H. Zhang, Y.H. Zhang, P. Liu, P. Wang, D. Wu, Y.L. Gao, Evolution of the electronic structure of $C_{60}/La_{0.67}Sr_{0.33}MnO_3$ interface, Appl. Phys. Lett. 108 (2016) 011603 https://aip.scitation.org/doi/10.1063/1.4939457.

[24] N. Liu, Q. Du, G.Z. Yin, P.F. Liu, L. Li, H.P. Xie, C. Zhu, Y.J. Li, H.P. Zhou, Q. Chen, Extremely low trap-state energy level perovskite solar cells passivated using NH_2-POSS with improved efficiency and stability, *J.* Mater. Chem. A. 6 (2018) 6806–6814 https://doi.org/10.1039/C7TA11345E.

[25] V.K. Ravi, P.K. Santra, N. Joshi, J. Chugh, S.K. Singh, H. Rensmo, P. Ghosh, A. Nag, Origin of the substitution mechanism for the binding of organic ligands on the surface of $CsPbBr_3$ perovskite nanocubes, J. Phys. Chem. Lett. 8 (2017) 4988–4994 https://doi.org/10.1021/acs.jpclett.7b02192.

[26] J. Endres, M. Kulbak, L.F. Zhao, B.P. Rand, D. Cahen, G. Hodes, A. Kahn, Electronic structure of the $CsPbBr_3$/polytriarylamine (PTAA) system, J. Appl. Phys. 121 (2017) 035304 https://doi.org/10.1063/1.4974471.

[27] X.L. Liu, C.G. Wang, I. Irfan, S.J. Yi, Y.L. Gao, Effect of oxygen plasma treatment on air exposed MoOx thin film, Org. Electron. 15 (2014) 977–983 https://doi.org/10.1016/j.orgel.2014.02.011.

[28] S. Colella, E. Mosconi, G. Pellegrino, A. Alberti, V.L. Guerra, P.S. Masi, A. Listorti, A. Rizzo, G.G. Condorelli, Elusive presence of chloride in mixed halide perovskite solar cells, J. Phys. Chem. Lett. 5 (2014) 3532–3538 https://doi.org/10.1021/jz501869f.

[29] L.P. Kazansky, I.A. Selyaninov, Yu I. Kuznetsov, Angle resolved XPS of mono-molecular layer of 5-chlorobenzotriazole on oxidized Metallic surface, Appl. Surf. Sci. 259 (2012) 385–392 https://doi.org/10.1016/j.apsusc.2012.07.056.